Insight into Nature of Iron Sulfide Surfaces during the Electrochemical Hydrogen Evolution and CO$_2$ Reduction Reactions

Siti N. A. Zakaria,[a,b] Nathan Hollingsworth,[a] Husn U. Islam,[a] Anna Roffey,[a] David Santos-Carballal,[c] Alberto Roldan,[c] Wim Bras,[d] Gopinathan Sankar,[a] Graeme Hogarth,[e] Katherine B. Holt,[a]* and Nora H. de Leeuw[a,c]*

a. Department of Chemistry, University College London, 20 Gordon St., London WC1H 0AJ, UK
b. Faculty of Science, Universiti Brunei Darussalam, Jln Tungku Link, Gadong BE1410, Brunei
c. School of Chemistry, Cardiff University, Main Building, Park Place, Cardiff, CF10 3AT, UK.
d. European Synchrotron Radiation Facility, BP220, Grenoble F38043, France.
e. Department of Chemistry, Kings College London, Britannia House, 7 Trinity St, London, SE1 1DB, UK.

*corresponding authors: k.b.holt@ucl.ac.uk, DeLeeuwN@cardiff.ac.uk

Table of Contents

SI1:   Synthesis and Characterisation of greigite

Oleylamine-capped Greigite was synthesised by thermal decomposition of $Fe(S_2CN^iBu_2)_3$ and $(Et_2NCS_2)_2$ in oleylamine at 230^oC. The sample was washed with methanol and dried under vacuum. The powder was then suspended in isopropanol for drop-coating onto the boron-doped diamond (BDD) electrode for cyclic voltammetry (CV) and *in situ* IR experiments. For XAS experiments greigite dispersed in a carbon nanoparticle matrix was used and drop-coated from chloroform onto the electrode. This was synthesised in the same way as pure greigite but with nano-carbon powder (Johnson Matthey) present in the reaction vessel.

The greigite particles were characterised by High Resolution Transmission Electron Microscopy (HRTEM) and found to be a plate-like morphology of average dimensions ca. 100 x 70 x 20 nm (Fig S1). The largest surfaces were {100} crystal plane and the edges {111}. XRD confirmed the samples were pure greigite. EXAFS analysis of the XAS spectrum gave Fe-S bond distances in agreement with calculated bond distances for greigite.
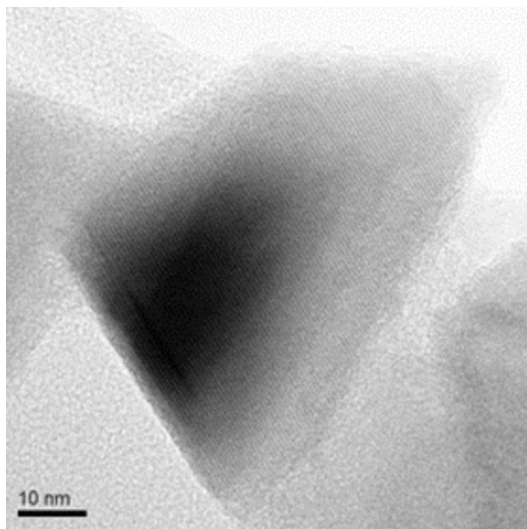

Figure S1: HRTEM image of as-synthesised greigite nanoplatelet.

SI2:   Description of *in situ* XAS experiments

XAS experiments using greigite-modified electrodes were carried out on the Dutch-Belgian beamline BM26A at the ESRF. Monochromatic radiation was supplied by a double Si(111) crystal. All *in situ* measurements were acquired in fluorescence mode using the 9 element germanium solid state detector. XAS measurements were acquired at the iron K-edge (7112 eV) and measurements were set so that each acquisition lasted *ca.* 20 minutes, thus providing three scans at each potential. A k range of 11 Å^{-1} was possible in this time frame.

An *in situ* cell was designed for this experiment, as shown in cross-section side profile in the main manuscript and in front profile in Figure S2 below. The distance of the 1 cm diameter working electrode from the 40 μm thick Kapton window could be adjusted using a screw and the window-electrode separation was kept constant at *ca.* 0.5 mm for the experiments reported in this paper. The counter electrode (CE) was a coiled Pt wire and reference electrode (RE) Ag / AgCl / KCl (sat). Potentials reported in the main manuscript have been converted to SHE. Potentials were controlled using a μ-Autolab potentiostat. Solutions were deoxygenated by bubbling for 20 mins with nitrogen, or saturated with high purity CO_2 gas.
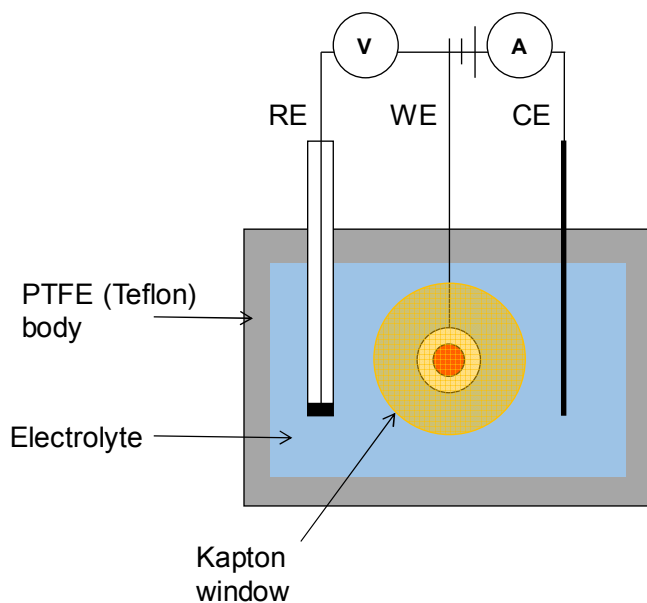

Figure S2: Schematic of in situ XAS electrochemical cell (not to scale), cross-section front view

SI3:   Analysis of XANES spectra

XAS data were normalized and background subtracted using Horea Athena. The XANES region was fit using Linear Combination Fitting (LCF) analysis, where the experimental spectrum is fit semi-quantitively with weighted contributions from the species that contribute to the final spectrum. Dry greigite, greigite with no potential applied and -0.05 V vs. SHE applied have XANES spectra that could be fit with the greigite standard only. When -0.6 V vs. SHE was applied, the sample was found to have contributions from oxide or hydroxide species (see main manuscript). Standard XANES spectra were measured for iron oxide and hydroxide species, as well as hydrated species such as $Fe(H_2O)^{2+/3+}$.

The best fits for the -0.6 V sample were obtained with contributions from greigite and goethite (α-FeOOH) standards, with % contribution values given in the manuscript. Figure S3 shows experimental XANES spectra (solid lines) and best fit spectra with a combination of greigite and goethite. Legend potential values are vs. Ag / AgCl / KCl (sat.). Note that only the -0.25 V (-0.05 V vs. SHE) and -0.8 V (-0.6 V vs. SHE) data are discussed in detail in the main text. After application of -0.8 V the spectra show that the hydroxide shell is maintained when the potential is cycled positive and then negative again, i.e. it is not stripped off. It should be noted that although a good fit was obtained with goethite, this is the anticipated final stable product from transformations of mixed valence iron hydroxide species, such as fougerite and green rusts, for which standards were not available. The actual hydroxide species present under experimental conditions is likely a mix of these intermediate species, but goethite was taken as an adequate standard for semi-quantitative analysis of the formation of the hydroxide shell.
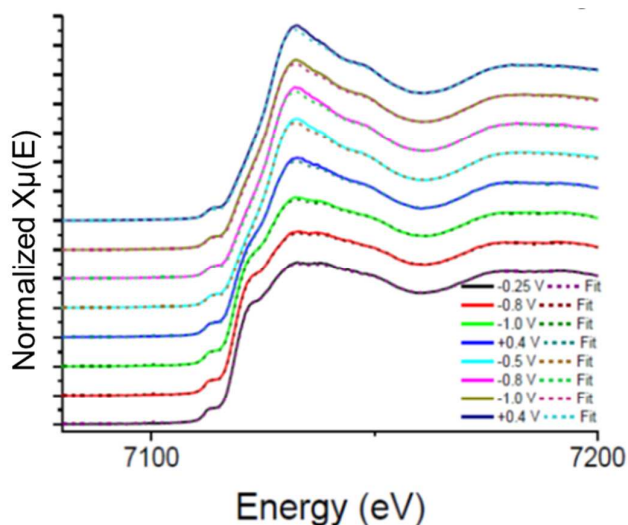

Figure S3: Experimental (bold lines) and LCF (dotted) XANES spectra for greigite in deoxygenated 0.1 M pH 6.8 phosphate buffer solution. Potentials in legend are vs. Ag / AgCl / KCl (sat).

SI4:   EXAFS analysis

In the best fit, EXAFS modelling of the dry greigite nanoparticles was 1.5 tetrahedral Fe-S at 2.18 Å, and 3.7 octahedral Fe-S at 2.38 Å. 0.3 Fe-O distances at 2.01 Å were implemented into the calculation to improve fitting and indicated a slight oxidation of the system. The analysis was performed on Excurve98 (Binsted N, EXCURV98: CCLRC Daresbury Laboratory computer program (1998)). Coordination remained fixed at calculated values while bond distance and Debye-Waller factor were varied. For the *in situ* electrochemistry data, EXAFS analysis is complicated by the wide range of possible coordination environments and oxidation states. For analysis of the EXAFS data in this case the relative contribution of Fe-S and Fe-O bonding obtained from the LCF of the XANES spectrum were used as the input parameters. Average Fe-S and Fe-O bond distances were kept constant where possible and coordination number was refined. For greigite samples held at -0.05 V and -0.6 V vs. SHE the following coordination numbers were obtained:

		Bond Length / 10^{-10} m	Coordination No
-0.05 V / N_2	Fe-O	1.95	0.4
	Fe-S (tet)	2.22	1.4
	Fe-S (oct)	2.39	2.0
-0.6 V / N_2	Fe-O	1.96	2.6
	Fe-S (tet)	2.21	0.9
	Fe-S (oct)	2.39	1.3

The EXAFS data supports the results from the XANES spectra: Fe-O coordination increases from 0.4 to 2.6 when a potential of -0.6 V is applied in deoxygenated solution. The Fourier Transform of the EXAFS is shown in Fig S4 below, where the shortening bond distance of the first shell is typical of the longer Fe-S distances converting to shorter Fe-O distance. This corroborates the interpretation of the XANES spectra as resulting from conversion of greigite to oxyhydroxide species.
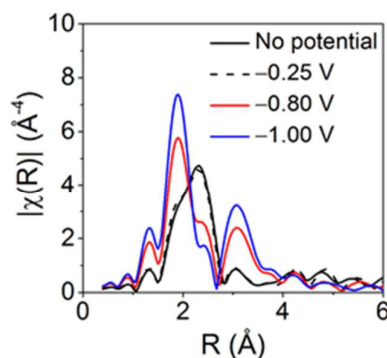

Figure S4: Fourier Transform of the EXAFS analysis

SI5: Ex situ S K-edges XANES

Ex situ sulfur K-edge XAS measurements were taken of carbon loaded greigite before (black) and after (purple) reduction to -0.8 V vs. SHE in a pH 6.8 phosphate buffer solution bubbled with N_2 (Fig S5). Interpretation of the XAS data requires comparison with spectra of standards. The first standard shown in Fig S5 is fresh hexagonal sheet greigite (blue) synthesised by the solvothermal decomposition of an iron dithiocarbamate precursor in oleylamine. The spectrum acts as a standard for S^{2-} with an edge jump at 2469 eV. There is also a broad feature between 2474 and 2482 eV which is characteristic of sulfide structures. Iron sulfite (green), iron sulfate (pink) and sulfonic acid (turquoise) are used as positively charged sulfur standards.
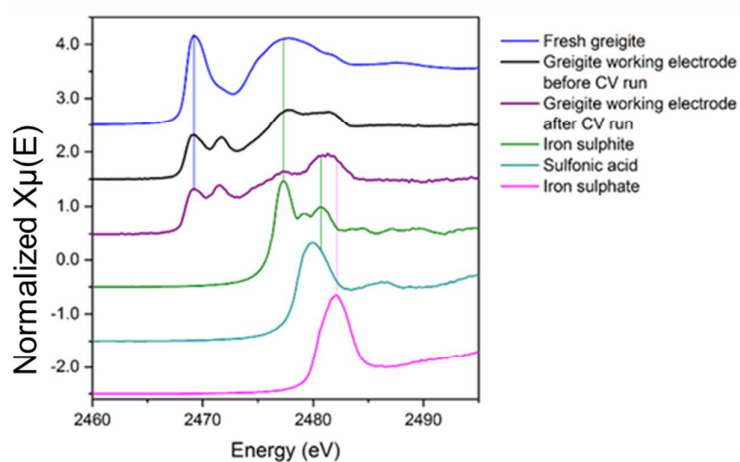

Figure S5: XANES spectra of greigite before and after electrochemical reduction using CV along with standards.

The carbon loaded greigite (black) shows a significant contribution from S_2^{2-} as well as S^{2-} species at its surface. Sulfide phases are known to transform over time to the most stable iron sulfide phase pyrite. The S_2^{2-} species is probably found closer to the surface which S k-edge is sensitive to since the Fe-S distance of pyrite at 2.26 Å is not observed on the more infiltrating Fe K-edge EXAFS of the same structure. The surface also shows traces of positively charged sulfur species. The spent greigite sample taken after being cycled to negative potentials has similar peaks at S^{2-} and S_2^{2-}, with a small decrease in S^{2-} species. Ratios of peaks in the positively charged sulfur region are more significantly changed. A large contribution from SO_4^{2-} is detected. As well as this, reduction in amount of sulfite species is observed. This data supports the Fe K-edge data showing the incorporation of oxygen into the structure. However it should be noted that the S K-edge data was obtained *ex situ*, so oxidation of the sample by air is difficult to avoid.

SI6: Description of in situ ATR IR spectroelectrochemistry experiment

A Bruker Tensor 27 IR spectrometer with a diamond crystal single-reflection internal reflection element ATR prism accessory was used for all experiments. The instrument is fitted with a room temperature DLaTGS detector at 4 cm^{-1} resolution. A schematic of the complete cell is shown in Figure S6 below. The working electrode is a boron-doped diamond (BDD) electrode with layer of greigite physisorbed on the surface by drop-coating. The distance between the bare BDD electrode and the ATR prism has been determined experimentally as *ca*. 17 μm and the greigite nanoparticle layer swells in solution to occupy the region between the electrode and the prism. The penetration depth of the IR evanescent wave is wavelength dependent, but less than 2 μm, so only the interface furthest from the electrode is probed. The counter electrode (CE) was a coiled Pt wire and the reference electrode (RE) was Ag / AgCl / KCl (sat). All potentials in the main manuscript have been converted to E vs. Standard Hydrogen Electrode (SHE) for easier comparison to Pourbaix diagrams. The potential was controlled with a Palmsens Emstat2 potentiostat (Palmsens, NL) running PSTrace (v3.0) software. The greigite-modified electrode was equilibrated in the electrolyte (deoxygenated for 20 min prior with Ar, or purged with high purity CO_2 for 20 min) for *ca*. 30 min then an IR background spectrum obtained. The potential of interest was applied and spectra recorded relative to the spectrum of the equilibrated sample. A single spectrum was computed by Fourier transformation of 100 averaged interferograms for background and sample and the software was programmed to record a spectrum every 300 seconds.
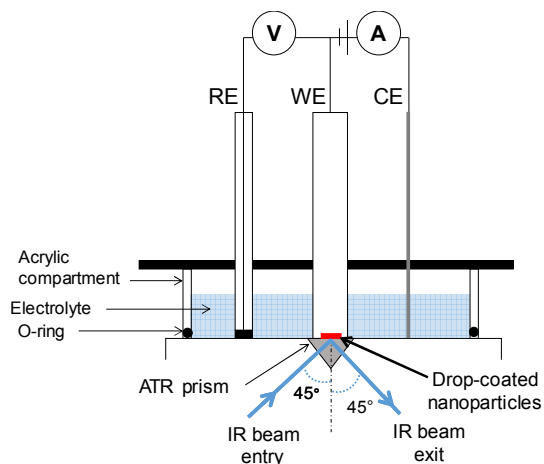

Figure S6: Schematic (not to scale) of the in situ ATR IR spectroelectrochemistry cell.

SI7:   Computational methods

Calculation details:

We have performed spin-polarized calculations with the Vienna Ab-initio Simulation Package (VASP).[1–4] All simulations were carried out within the periodic plane-wave DFT framework. The projector augmented wave (PAW) method was used to describe the core electrons and their interaction with the valence ones.[5,6] The frozen core of the Fe, S, P O and C elements was defined up to and including the $3p$, $2p$, $2p$, $1s$ and $1s$ electrons, respectively. At the level of the generalized gradient approximation (GGA), the exchange-correlation in the form of the Perdew-Wang 91 (PW91)[7,8] functional was used together with the spin interpolation of Vosko *et al.*[9] The long-range dispersion interactions were added via the semi-empirical method of Grimme (D2),[10] using the global scaling factor parameter optimized for the Perdew-Burke-Ernzerhof (PBE)[11,12] functional, $s_6 = 0.75$, which has shown to provide good results in the modelling of a number of sulfides.[13–18] Brillouin zone integrations of the surface slabs were performed using a Γ-centred Monkhorst-Pack grid[19] of $4\times4\times1$ and $5\times5\times1$ k-points for the {100} and {111} surfaces, respectively. The bulk of Fe_3S_4 was simulated using the conventional spinel cubic unit cell[20] and the elemental sulphur was modelled as the orthorhombic polymorph of S_8, using the primitive triclinic crystal structure containing 32 atoms.[21] We chose a k-points spacing of $4\times4\times4$ and $7\times7\times7$ for the bulk calculations of Fe_3S_4 and S_8, respectively. The isolated O_2, H_2O, H_3PO_4 and CO_2 molecules and the O atom were modelled in a cell with broken symmetry which was big enough to avoid intermolecular interactions, sampling only the Γ point of the Brillouin zone. In order to increase the integration efficiency in the reciprocal space, the partial occupancies for all calculations of the condensed phases were determined using the tetrahedron method with Blöchl corrections,[22] while we used the Gaussian smearing technique and 0.02 eV for the width of the smearing for the simulations of the isolated molecules and atoms. Kohn-Sham (KS) valence states were expanded in a plane-wave basis set with the kinetic energy's cut-off fixed at 600 eV. The DFT + U[23] version of Dudarev *et al.*[24] was used for the description of the localized and strongly correlated Fe d electrons. Based on previous work, we have chosen a U_{eff} of 1.0 eV.[25–28] Electronic density optimization was stopped when the total energy difference between two consecutive self-consistent loop steps was below 10^{-5} eV. Atomic positions were relaxed to their ground state using the conjugate-gradient method and were considered converged when the Hellmann-Feynman forces on all atoms were smaller than 0.02 eV·Å^{-1}. Surface calculations were carried out using symmetric and non-dipolar stoichiometric slabs. More details about the surface slab models can be found elsewhere.[28–30] Vibrational infrared frequencies were determined for the adsorbed species on the greigite surfaces using the central finite differences method. In order to calculate the oxidation energies (E_{oxid}) of the bulk and surfaces of Fe_3S_4, we have considered the

process of replacement of one sulphur (forming orthorhombic S_8) by one oxygen atom (from the O_2 gas phase molecule) according to the following equation,

$$E_{oxid} = E\left(Fe_{24}S_{31}O(s)\right) + \frac{1}{8}E\left(S_8(s)\right) - E\left(Fe_{24}S_{32}(s)\right) - \frac{1}{2}E\left(O_2(g)\right) \qquad (1)$$

where $E\left(Fe_{24}S_{31}O(s)\right)$ is the energy of a partially oxidised Fe_3S_4 bulk or surface slab, $E\left(S_8(s)\right)$ is the energy of a single sulphur atom in the orthorhombic crystal structure, $E\left(Fe_{24}S_{32}(s)\right)$ is the energy of Fe_3S_4 bulk or its pristine surface slab and $\frac{1}{2}E\left(O_2(g)\right)$ is the energy of half of the oxygen molecule corrected with half of the overbinding of the O_2 molecule. Further details about the correction of the overbinding of the O_2 molecule can be found in Ref [31].

Binding energies (BE), were calculated as

$$BE = E_{surf+adsorb} - E_{surf} - E_{adsorb} \qquad (2)$$

where $E_{surf+adsorb}$ is the energy of the surface slab with the adsorbed species, E_{surf} is the energy of the pristine surface slab and E_{adsorb} is the energy of the isolated adsorbate molecule.

SI8:   EDX analysis of greigite particles after electrochemical cycling

A carbon rod modified with a drop-coated layer of greigite was cycled between 0.2 and -0.8 V vs. SHE in deoxygenated pH 6.8 phosphate buffer solution. The electrode was removed from solution, dried rapidly under argon and stored in a vacuum desiccator. The dried powder was scraped from the rod and analysed using HRTEM (see main document, Fig 6) and EDX (Figure S7). Figure S7 shows EDX elemental analysis through the region of the yellow line indicated in the image. The dark black region is the nanoparticle imaged by HRTEM and shown in Fig 6 in the main manuscript. The surrounding grey area is the TEM grid. Fe, S and O are present in the region of the nanoparticle, indicating that the greigite particle has oxygen content. The relative concentration of oxygen is higher at the edges of the particle which is consistent with the appearance of the amorphous layer that we have attributed to Fe hydroxides.
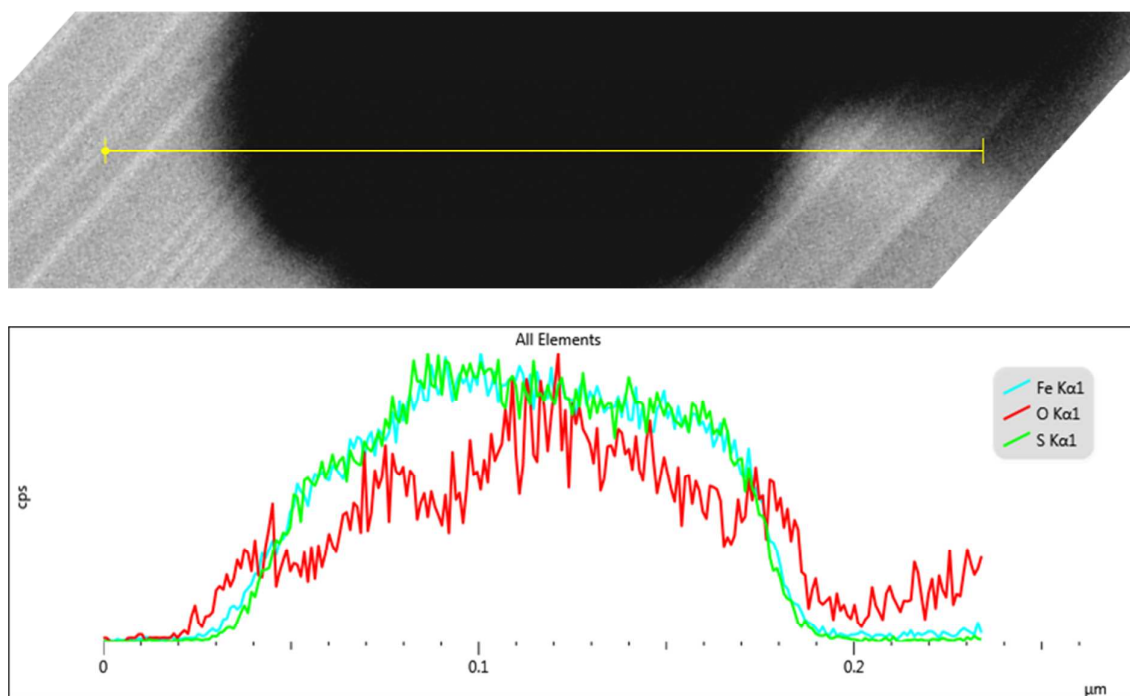

Figure S7: EDX elemental analysis of Fe, S and O content of line section through cycled greigite nanoparticle. Yellow line in top image shows line analysed. Black feature in image is nanoparticle, grey is TEM grid.

SI9: XRD analysis of greigite particles after electrochemical cycling

A carbon rod modified with a drop-coated layer of greigite was cycled between 0.2 and -0.8 V vs. SHE in deoxygenated pH 6.8 phosphate buffer solution. The electrode was removed from solution, dried rapidly under argon and stored in a vacuum desiccator. The dried powder was scraped from the rod and analysed by XRD. As seen in Fig S8 the XRD pattern shows a good match for greigite indicating the crystalline core is intact after cycling. There is no evidence for crystalline oxide or hydroxide in the sample.
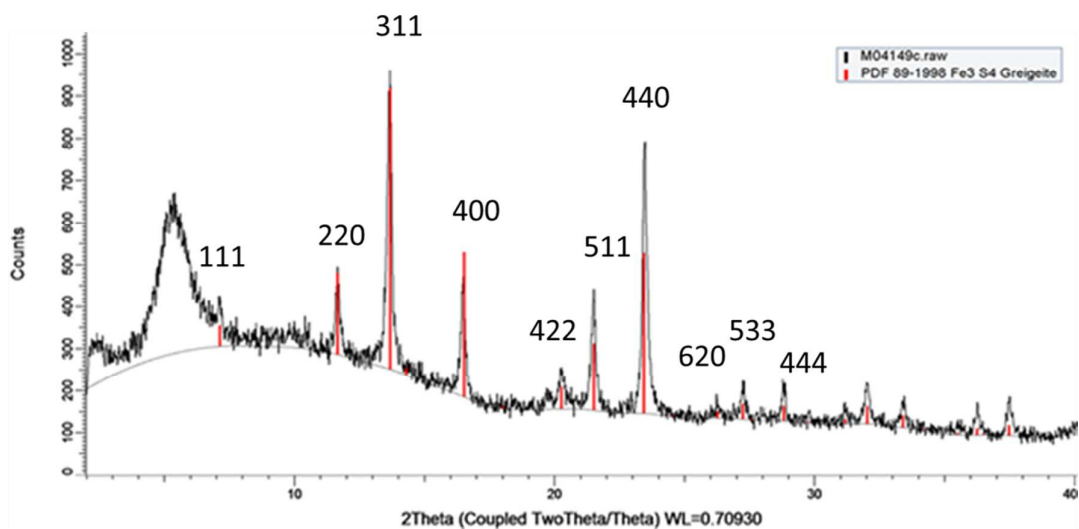

Figure S8: Experimental XRD pattern for cycled greigite powder from electrode, with red lines showing fit to greigite structure.

SI10: Cyclic voltammogram (CV) of greigite modified electrode in CO_2 saturated solution
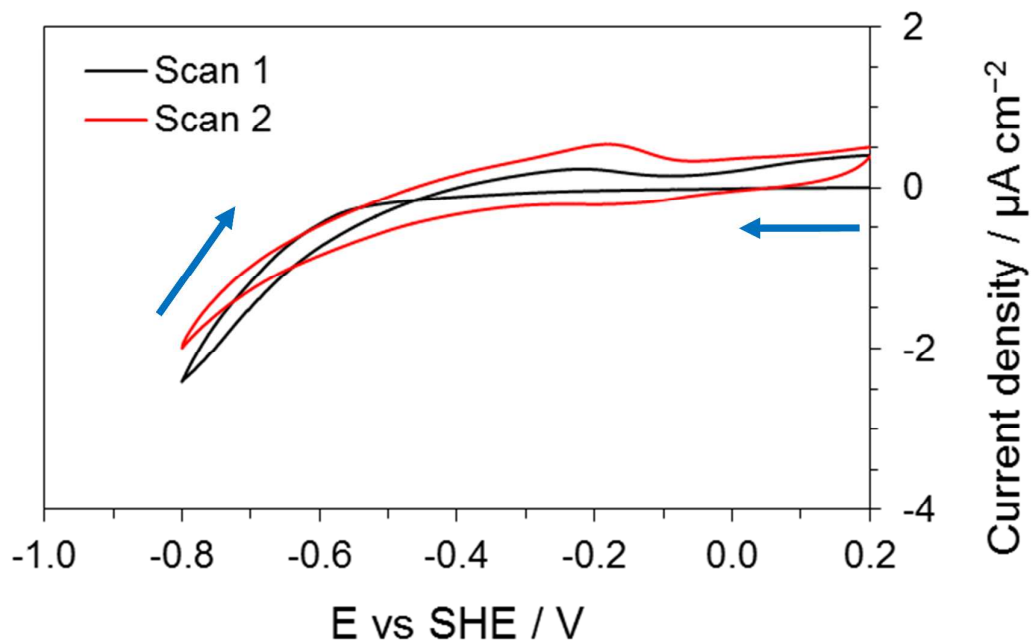

Figure S9: First and second CV scan of greigite modified electrode in CO_2 saturated pH 6.8 phosphate buffer solution (0.1 M K_2HPO_4 / 0.1 M KH_2PO_4, final pH = 6.5). Scan rate 0.01 V s^{-1}. Features are the same as those in deoxygenated solution (see main manuscript) but currents are three orders of magnitude lower.

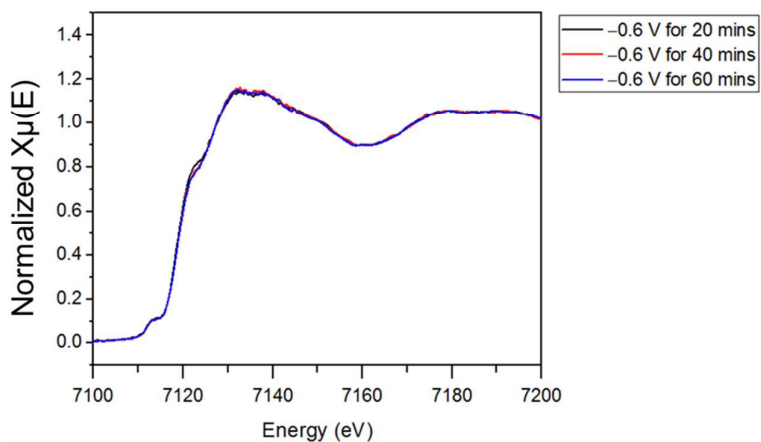**SI11:   XANES spectra and EXAFS analysis of greigite in CO$_2$ saturated solution**

Figure S10: XANES spectra of greigite-modified electrode in CO$_2$ saturated pH 6.8 phosphate buffer solution (0.1 M K$_2$HPO$_4$ / 0.1 M KH$_2$PO$_4$, final pH = 6.5) after 20 min, 40 min and 60 min.

EXAFS analysis was carried out as described in section SI4, with the following parameters obtained:

		Bond Length / 10^{-10} m	Coordination No
-0.6 V / CO$_2$	Fe-O	1.99	1.1
	Fe-S (tet)	2.21	1.2
	Fe-S (oct)	2.39	3.0

The EXAFS data supports the results from the XANES spectra: When the solution is saturated with CO2 the Fe-O coordination number only increases to 1.1 compared to 2.6 in deoxygenated solution.

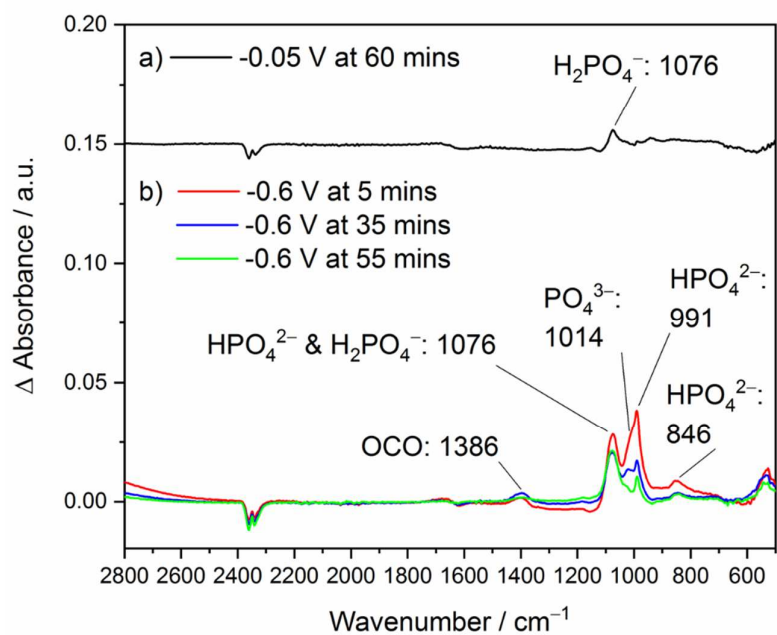**SI12: In situ IR spectroelectrochemistry in CO$_2$ saturated solution**

Figure S11: In situ IR spectra obtained in CO$_2$ saturated 0.1 M K$_2$HPO$_4$/KH$_2$PO$_4$ solution

SI13:   References

(1)   Kresse, G.; Hafner, J. Ab Initio Molecular Dynamics for Liquid Metals. *Phys. Rev. B* **1993**, *47*, 558–561.

(2)   Kresse, G.; Hafner, J. Ab Initio Molecular-Dynamics Simulation of the Liquid-Metal–amorphous-Semiconductor Transition in Germanium. *Phys. Rev. B* **1994**, *49*, 14251–14269.

(3)   Kresse, G.; Furthmüller, J. Efficiency of Ab-Initio Total Energy Calculations for Metals and Semiconductors Using a Plane-Wave Basis Set. *Comput. Mater. Sci.* **1996**, *6*, 15–50.

(4)   Kresse, G.; Furthmüller, J. Efficient Iterative Schemes for Ab Initio Total-Energy Calculations Using a Plane-Wave Basis Set. *Phys. Rev. B* **1996**, *54*, 11169–11186.

(5)   Kresse, G.; Joubert, D. From Ultrasoft Pseudopotentials to the Projector Augmented-Wave Method. *Phys. Rev. B* **1999**, *59*, 1758–1775.

(6)   Blöchl, P. E. Projector Augmented-Wave Method. *Phys. Rev. B* **1994**, *50*, 17953–17979.

(7)   Perdew, J. P.; Chevary, J. A.; Vosko, S. H.; Jackson, K. A.; Pederson, M. R.; Singh, D. J.; Fiolhais, C. Atoms, Molecules, Solids, and Surfaces: Applications of the Generalized Gradient Approximation for Exchange and Correlation. *Phys. Rev. B* **1992**, *46*, 6671–6687.

(8)   Perdew, J. P.; Chevary, J. A.; Vosko, S. H.; Jackson, K. A.; Pederson, M. R.; Singh, D. J.; Fiolhais, C. Erratum: Atoms, Molecules, Solids, and Surfaces: Applications of the Generalized Gradient Approximation for Exchange and Correlation [Phys. Rev. B 46, 6671 (1992)]. *Phys. Rev. B* **1993**, *48*, 4978–4978.

(9)   Vosko, S. H.; Wilk, L.; Nusair, M. Accurate Spin-Dependent Electron Liquid Correlation Energies for Local Spin Density Calculations: A Critical Analysis. *Can. J. Phys.* **1980**, *58*, 1200–1211.

(10)   Grimme, S. Semiempirical GGA-Type Density Functional Constructed with a Long-Range Dispersion Correction. *J. Comput. Chem.* **2006**, *27*, 1787–1799.

(11)   Perdew, J. P.; Burke, K.; Ernzerhof, M. Generalized Gradient Approximation Made Simple [Phys. Rev. Lett. 77, 3865 (1996)]. *Phys. Rev. Lett.* **1997**, *78*, 1396–1396.

(12)   Perdew, J. P.; Burke, K.; Ernzerhof, M. Generalized Gradient Approximation Made Simple. *Phys. Rev. Lett.* **1996**, *77*, 3865–3868.

(13)   Terranova, U.; de Leeuw, N. H. Aqueous Fe_2S_2 Cluster: Structure, Magnetic Coupling, and Hydration Behaviour from Hubbard U Density Functional Theory. *Phys. Chem. Chem. Phys.* **2014**, *16*, 13426–13433.

(14)   Dzade, N. Y.; Roldan, A.; de Leeuw, N. H. The Surface Chemistry of NO_x on Mackinawite (FeS) Surfaces: A DFT-D2 Study. *Phys. Chem. Chem. Phys.* **2014**, *16*, 15444–15456.

(15)   Santos-Carballal, D.; Roldan, A.; Grau-Crespo, R.; de Leeuw, N. H. First-Principles Study of the

Inversion Thermodynamics and Electronic Structure of FeM_2X_4 (Thio)Spinels (M = Cr, Mn, Co, Ni; X = O, S). *Phys. Rev. B* **2015**, *91*, 195106.

(16)   Haider, S.; Roldan, A.; De Leeuw, N. H. Catalytic Dissociation of Water on the (001), (011), and (111) Surfaces of Violarite, FeNi$_2$S$_4$: A DFT-D2 Study. *J. Phys. Chem. C* **2014**, *118*, 1958–1967.

(17)   Dzade, N. Y.; Roldan, A.; de Leeuw, N. H. Adsorption of Methylamine on Mackinawite (FES) Surfaces: A Density Functional Theory Study. *J. Chem. Phys.* **2013**, *139*, 124708.

(18)   Dzade, N. Y.; Roldan, A.; de Leeuw, N. H. Activation and Dissociation of CO_2 on the (001), (011), and (111) Surfaces of Mackinawite (FeS): A Dispersion-Corrected DFT Study. *J. Chem. Phys.* **2015**, *143*, 094703.

(19)   Monkhorst, H. J.; Pack, J. D. Special Points for Brillouin-Zone Integrations. *Phys. Rev. B* **1976**, *13*, 5188–5192.

(20)   Skinner, B. J.; Erd, R. C.; Grimaldi, F. S. Greigite, the Thio-Spinel of Iron; a New Mineral. *Am. Mineral.* **1964**, *49*, 543–555.

(21)   Cameron, T. S.; Decken, A.; Dionne, I.; Fang, M.; Krossing, I.; Passmore, J. Approaching the Gas-Phase Structures of $[AgS_8]^+$ and $[AgS_{16}]^+$ in the Solid State. *Chem. - A Eur. J.* **2002**, *8*, 3386–3401.

(22)   Blöchl, P. E.; Jepsen, O.; Andersen, O. K. Improved Tetrahedron Method for Brillouin-Zone Integrations. *Phys. Rev. B* **1994**, *49*, 16223–16233.

(23)   Anisimov, V. I.; Korotin, M. A.; Zaanen, J.; Andersen, O. K. Spin Bags, Polarons, and Impurity Potentials in La$_{2-x}$Sr$_x$CuO$_4$ from First Principles. *Phys. Rev. Lett.* **1992**, *68*, 345–348.

(24)   Dudarev, S. L.; Botton, G. A.; Savrasov, S. Y.; Humphreys, C. J.; Sutton, A. P. Electron-Energy-Loss Spectra and the Structural Stability of Nickel Oxide: An LSDA+U Study. *Phys. Rev. B* **1998**, *57*, 1505–1509.

(25)   Devey, A. J.; Grau-Crespo, R.; de Leeuw, N. H. Electronic and Magnetic Structure of Fe$_3$S$_4$: GGA+U Investigation. *Phys. Rev. B* **2009**, *79*, 195126.

(26)   Roldan, A.; Santos-Carballal, D.; de Leeuw, N. H. A Comparative DFT Study of the Mechanical and Electronic Properties of Greigite Fe$_3$S$_4$ and Magnetite Fe$_3$O$_4$. *J. Chem. Phys.* **2013**, *138*, 204712.

(27)   Haider, S.; Grau-Crespo, R.; Devey, A. J.; de Leeuw, N. H. Cation Distribution and Mixing Thermodynamics in Fe/Ni Thiospinels. *Geochim. Cosmochim. Acta* **2012**, *88*, 275–282.

(28)   Roldan, A.; Hollingsworth, N.; Roffey, A.; Islam, H.-U.; Goodall, J. B. M.; Catlow, C. R. A.; Darr, J. A.; Bras, W.; Sankar, G.; Holt, K. B.; Hogarth, G.; de Leeuw, N. H. Bio-Inspired CO_2 Conversion by Iron Sulfide Catalysts under Sustainable Conditions. *Chem. Commun.* **2015**, *51*, 7501–7504.

(29) Santos-Carballal, D.; Roldan, A.; de Leeuw, N. H. Early Oxidation Processes on the Greigite Fe$_3$S$_4$(001) Surface by Water: A Density Functional Theory Study. *J. Phys. Chem. C* **2016**, *120*, 8616–8629.

(30) Roldan, A.; de Leeuw, N. H. Catalytic Water Dissociation by Greigite Fe$_3$S$_4$ Surfaces: Density Functional Theory Study. *Proc. R. Soc. A Math. Phys. Eng. Sci.* **2016**, *472*, 20160080.

(31) Santos-Carballal, D.; Roldan, A.; Grau-Crespo, R.; de Leeuw, N. H. A DFT Study of the Structures, Stabilities and Redox Behaviour of the Major Surfaces of Magnetite Fe$_3$O$_4$. *Phys. Chem. Chem. Phys.* **2014**, *16*, 21082–21097.